

Influence of subband mixing, due to spin-orbit interaction, on the transmission through periodically modulated waveguides

X. F. Wang[†] and P. Vasilopoulos^{*}

Concordia University Department of Physics

1455 de Maisonneuve Ouest

Montréal, Québec, H3G 1M8, Canada

(Dated: April 12, 2018)

Abstract

Ballistic spin transport, through periodically stubbed waveguides, is studied in the presence of a weak spin-orbit interaction (SOI) and the resulting subband mixing. By an appropriate choice of the waveguide length and of the stub parameters injected spin-polarized electrons can be blocked completely and the transmission shows a periodic and nearly square-wave pattern with wide gaps when only one mode is allowed to propagate in the waveguide. Relative to the case when subband mixing is neglected, the transmission changes drastically as a function of the incident electron energy or of the stub height, as it exhibits new peaks or dips, but remains robust as a function of the stubs' degree of asymmetry. Varying the strength of the SOI parameter changes the relative contribution to the total transmission or conductance of the spin-up and spin-down states. The structure considered is a reasonable candidate for establishing a spin transistor.

PACS numbers: 72.20.-i, 72.30.+q, 73.20.Mf

I. INTRODUCTION

Recently research in spin-related effects, such as spin injection into devices, spin-polarized transport, etc., has been intensified. Part of the reason is that the possibility exists to use the electron's spin for quantum computations [3]. The basic principle of a spin transistor was formulated in Ref. [4] for a waveguide in the presence of the spin-orbit interaction (SOI) or Rashba coupling [5] and was recently studied for a simple semiconductor waveguide using a tight-binding model [6] or periodically modulated waveguides [7]. Various spin-filtering [8] or spin-valve [9] effects have been studied and several designs have been proposed to spin-polarize electronic currents in nanostructures [8, 10] among other studies of SOI effects on the band structure and transport of similar systems [11, 12]. In this respect several efforts have been made using ferromagnet-semiconductor interfaces to produce spin-polarized electrons, but this method must face the mismatch of physical parameters between these two quite different materials [13]. Another idea is to employ diluted magnetic semiconductors (DMS), which can match well with other extensively used semiconductors like AlGaAs, and has created a lot of interest in DMS [14, 15].

Spin degeneracy in semiconductors results from inversion symmetry, in space and time, of the considered system. By introducing a spatial inversion asymmetry, one can realize spin splitting for carriers of finite momentum without applying any external magnetic field. This so-called Rashba effect or spin-orbit interaction (SOI) [5, 16] has been confirmed experimentally in various semiconductor structures [17]. In semiconductor heterostructures this spatial inversion asymmetry can be easily obtained by either built-in and external electric fields or by the position-dependent band edges. It is found that in many cases, especially in narrow gap semiconductor structures, the corresponding SOI is a linear function of the electronic momentum \mathbf{k} expressed as the Rashba term $\vec{\sigma} \cdot (\mathbf{k} \times \mathbf{E})$ in the electron Hamiltonian, where $\vec{\sigma}$ is the Pauli spin matrix and \mathbf{E} the local electric field. Thus, a local electric field \mathbf{E} acts on the electronic spin like a local magnetic field perpendicular to the directions of \mathbf{E} and of the electron momentum. The Rashba parameter is proportional to the average value of \mathbf{E} and can be well controlled by a top (back) gate over (below) the device [18].

Ballistic *spinless* electronic transport has been studied extensively in systems of reduced dimensionality [19, 20] but until recently it was not known how to effectively control the spin-polarized flux in the relevant systems. In previous work [7] we showed how spin-

polarized transport can be realized and controlled in stubbed waveguides mostly when only spin-up or spin-down electrons are injected and only one mode propagates in the waveguide. Our treatment, which showed how a *square-wave* and spin-dependent transmission could be realized, relied on the weakness of the SOI and the neglect of subband mixing due to this interaction. This put some constraints on the ranges of various parameters, namely the width of the waveguide, the height of the attached stubs, and the energy of the incident electrons. In the present paper we build upon this work and study in detail the effects of subband mixing which, to our knowledge, have been dealt with only partly in Ref. [6] for waveguides without stubs. In doing so we relax substantially the constraints mentioned above. Again our aim is to investigate in detail the conditions for the realization of a spin transistor in periodically stubbed semiconductor waveguides in the presence of SOI. As will be shown, we find new results (peaks or dips) in the transmission as a function of the incident electron energy or of the stub height, but its square-wave pattern, as a function of the stubs' degree of asymmetry, remains robust.

In Sec. II we present the formalism and contrast the results for the eigenvalues and eigenvectors with those obtained without subband mixing. In Sec. III we formulate the transmission problem and in Sec. IV we present numerical results. Concluding remarks follow in Sec. V.

II. FORMALISM

When a typical two-dimensional (2D) electronic system, such as an InGaAs/InAlAs quantum well, is confined, e.g., by a potential $V(x)$ along the x direction, we have a quasi-one-dimensional (Q1D) electronic system such as the stubbed waveguide shown in Fig. 1. The one-electron Hamiltonian, including the Rashba SOI term, reads

$$H = \frac{\vec{p}^2}{2m^*} + \frac{\alpha}{\hbar}(\vec{\sigma} \times \vec{p})_z + V(x) = \begin{bmatrix} -\lambda\vec{\nabla}^2 + V(x) & \alpha\nabla^- \\ -\alpha\nabla^+ & -\lambda\vec{\nabla}^2 + V(x) \end{bmatrix}, \quad (1)$$

where $\lambda = \hbar^2/2m^*$, $\vec{\nabla}^2 = \partial^2/\partial x^2 + \partial^2/\partial y^2$, and $\nabla_{\pm} = \partial/\partial x \pm i\partial/\partial y$. The parameter α measures the strength of the SOI and is proportional to the interface electric field; $\vec{\sigma} = (\sigma_x, \sigma_y, \sigma_z)$ denotes the spin Pauli matrices, and \vec{p} is the momentum operator. The wave

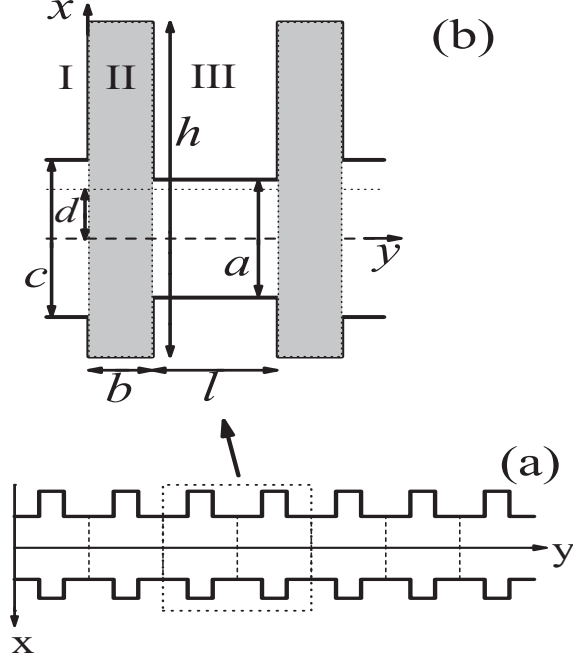


FIG. 1: A stubbed waveguide along the y direction (a) with a two-stub section detailed in (b). The width is c in region I and a in region III. The height of the stubs is h , their length b , and the length between them l . The asymmetry parameter d is the distance between the centerline of the waveguide and stubs.

function can be expressed in the form

$$\Psi_{k_y}(\mathbf{r}) = e^{ik_y y} \sum_{n\sigma} \phi_n(x) C_n^\sigma |\sigma\rangle = e^{ik_y y} \sum_n \phi_n(x) \begin{pmatrix} C_n^+ \\ C_n^- \end{pmatrix}, \quad (2)$$

with $|\sigma\rangle = \begin{pmatrix} 1 \\ 0 \end{pmatrix}$ for spin up (+) and $\begin{pmatrix} 0 \\ 1 \end{pmatrix}$ for spin down (-). $\phi(x)$ is the eigenfunction of the 1D Hamiltonian $h(x) = -\lambda \nabla_x^2 + V(x)$ with an assumed square-well confining potential $V(x)$.

We insert this eigenfunction in the equation $H\Psi = E\Psi$, multiply both sides by $\phi_m(x)$, and integrate over x . With $\int dx \phi_m(x) \phi_n(x) = \delta_{mn}$ and $J_{mn} = \int dx \phi_m(x) \phi'_n(x)$ we obtain

$$\begin{bmatrix} E_m^0 - E & \alpha k_y \\ \alpha k_y & E_m^0 - E \end{bmatrix} \begin{pmatrix} C_m^+ \\ C_m^- \end{pmatrix} + \alpha \sum_n J_{mn} \begin{bmatrix} 0 & 1 \\ -1 & 0 \end{bmatrix} \begin{pmatrix} C_n^+ \\ C_n^- \end{pmatrix} = 0, \quad (3)$$

where $E_m^0 = E_m + \lambda k_y^2$; the index m labels the discrete subbands resulting from the confinement along the x axis.

As shown elsewhere [7], if we neglect mixing between the subbands by assuming $J_{mn} \approx 0$, we can easily solve Eq. (3). This procedure is valid for $|\alpha J_{mn}| \ll |E_m - E_n|$. The resulting eigenvalues read

$$E^\pm(k_y) = E_m + \hbar^2 k_y^2 / 2m^* \pm \alpha k_y. \quad (4)$$

The eigenvectors corresponding to E^+, E^- satisfy $C_m^+ = \pm C_m^-$. Accordingly, the spin eigenfunctions can be taken as

$$|\pm\rangle = \begin{pmatrix} 1 \\ \pm 1 \end{pmatrix} / \sqrt{2}. \quad (5)$$

An important aspect in this case is that the difference in wave vectors k_y^+ and k_y^- , resulting from $E^+ = E^- = E$, is constant: it reads

$$k_y^- - k_y^+ = 2m^* \alpha / \hbar^2. \quad (6)$$

To go beyond this limiting case, described by $J_{mn} \approx 0$, and still have a tractable problem, we neglect all J_{mn} terms except J_{21} and $J_{12} = -J_{21} = 8/3w = \delta$, where w is the width of the waveguide along x . That is, we include mixing only between the first and second subband.

Then the secular equation for these two lowest subbands reads

$$\begin{bmatrix} E_1^0 - E & \alpha k_y & 0 & \alpha \delta \\ \alpha k_y & E_1^0 - E & -\alpha \delta & 0 \\ 0 & -\alpha \delta & E_2^0 - E & \alpha k_y \\ \alpha \delta & 0 & \alpha k_y & E_2^0 - E \end{bmatrix} \begin{pmatrix} C_1^+ \\ C_1^- \\ C_2^+ \\ C_2^- \end{pmatrix} = 0. \quad (7)$$

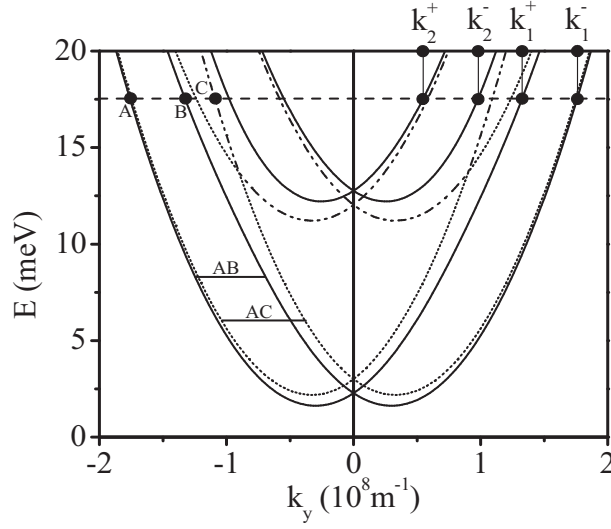


FIG. 2: Energy dispersion of the two lowest subbands, E_1 and E_2 , in a InGaAs waveguide 500Å wide. The solid curves include subband mixing, induced by the SOI, the dotted and dash-dotted ones do not. The intersections of the dispersion curves with the dashed line, showing the constant energy of the incident electrons, defines the \pm components of the wave vectors.

The resulting eigenvalues (ε_n^σ) and eigenvectors (Ψ_n^σ) are

$$\left\{ \begin{array}{ll} \varepsilon_1^+ = (E_1^0 + E_2^0 - \Delta E_-)/2, & \Psi_1^+ = \frac{1}{C} \begin{pmatrix} \phi_1 + r_B \phi_2 \\ \phi_1 - r_B \phi_2 \end{pmatrix}, \\ \varepsilon_1^- = (E_1^0 + E_2^0 - \Delta E_+)/2, & \Psi_1^- = \frac{1}{D} \begin{pmatrix} -\phi_1 + r_A \phi_2 \\ \phi_1 + r_A \phi_2 \end{pmatrix}, \\ \varepsilon_2^+ = (E_1^0 + E_2^0 + \Delta E_+)/2, & \Psi_2^+ = \frac{1}{D} \begin{pmatrix} \phi_2 + r_A \phi_1 \\ \phi_2 - r_A \phi_1 \end{pmatrix}, \\ \varepsilon_2^- = (E_1^0 + E_2^0 + \Delta E_-)/2, & \Psi_2^- = \frac{1}{C} \begin{pmatrix} -\phi_2 + r_B \phi_1 \\ \phi_2 + r_B \phi_1 \end{pmatrix}, \\ \varepsilon_n^+ = E_n^0 + \alpha k_y, & n > 2; \quad \Psi_n^+ = \frac{1}{\sqrt{2}} \begin{pmatrix} \phi_n \\ \phi_n \end{pmatrix}, \\ \varepsilon_n^- = E_n^0 - \alpha k_y, & n > 2; \quad \Psi_n^- = \frac{1}{\sqrt{2}} \begin{pmatrix} -\phi_n \\ \phi_n \end{pmatrix}. \end{array} \right. \quad (8)$$

Here $\Delta E_{\pm} = [(\Delta E_{12} \pm 2\alpha k_y)^2 + 4\alpha^2 \delta^2]^{1/2}$, $\Delta E_{12} = E_2^0 - E_1^0$, $A = (\Delta E_{12} + 2\alpha k_y) + \Delta E_+$, $B = (\Delta E_{12} - 2\alpha k_y) + \Delta E_-$, $r_A = 2\alpha\delta/A$, $r_B = 2\alpha\delta/B$, $D^2 = 2 + 2r_A^2$, and $C^2 = 2 + 2r_B^2$. Notice that the first four *two-row* eigenvectors are linear combinations of the *four-row* ones corresponding to Eq. (6). We further notice that the eigenvalues and eigenvectors given above reduce to those given, respectively, by Eqs. (4) and (5) if we set $\delta = 0$.

The dispersion relation given by Eq. (8) for the lowest two subbands is shown in Fig.

2 by the solid curves. For an electron of energy E in branches ε_1^+ , ε_1^- , ε_2^+ , and ε_2^- , the corresponding wave vectors along y are k_1^+ ($-k_1^-$), k_1^- ($-k_1^+$), k_2^+ ($-k_2^-$), and k_2^- ($-k_2^+$), respectively. When an electron with a positive wave vector k_y has an energy much higher than $E_c = 5E_1/2 + 9\hbar^2 E_1^2/(8m^* \alpha^2)$, the value at which anticrossing due to the SOI occurs between the ε_1^+ and the ε_2^- branches, its spin is up along the x direction ($|\sigma\rangle = \begin{pmatrix} 1 \\ 1 \end{pmatrix}$) when it is in the two higher spin branches (ε_2^+ , and ε_2^-) and down ($|\sigma\rangle = \begin{pmatrix} 1 \\ -1 \end{pmatrix}$) when it is in the other two branches. When its energy is lower than E_c , its spin is up in the "+" branches (ε_1^+ , and ε_2^+) and down in the "-" branches. Electrons of the same energy and the same but opposite momentum have always opposite spin orientation. Similar observations were made in Ref. [12] for a quantum wire with parabolic confinement. One interesting case is that an electron of positive momentum always has its spin pointing down and vice versa in the bag of each branch ε_n^σ with energy between the bottom of the branch and zero-momentum energy ε_n^0 . Another noteworthy feature in Fig. 2 is that mode mixing makes the wave vector differences $k_1^+ - k_1^-$ and $k_2^+ - k_2^-$ depend slightly on the energy. The length of the horizontal segment AC between the dotted curves, given by Eq. (6), is constant and independent of the energy whereas that of the segment AB between the solid curves is not and depends on the energy; AB satisfies Eq. (6) only approximately.

III. FORMULATION OF THE TRANSMISSION PROBLEM

Let us consider the transmission process when an electron of energy E is incident from the left to a stubbed waveguide shown in Fig. 1. The electron wave function is decomposed into "+" and "-" branches in all regions in Fig. 1. In each region we have $\phi_n(x) = \sin(n\pi(x + w/2)/w)$, $0 \leq x \leq w$, where w is the width along the x direction. Including spin and referring to Fig. 2, we can write the eigenfunction of energy E in region I as

$$\begin{aligned} \phi_1 = & \sum_m [c_m \Psi_{mc}^+(\eta_m^+) e^{i\eta_m^+ y} + \bar{c}_m \Psi_{mc}^+(-\eta_m^-) e^{-i\eta_m^- y} \\ & + d_m \Psi_{mc}^-(\eta_m^-) e^{i\eta_m^- y} + \bar{d}_m \Psi_{mc}^-(-\eta_m^+) e^{-i\eta_m^+ y}], \end{aligned} \quad (9)$$

in region III as

$$\begin{aligned} \phi_2 = & \sum_m [a_m \Psi_{ma}^+(\beta_m^+) e^{i\beta_m^+(y-b)} + \bar{a}_m \Psi_{ma}^+(-\beta_m^-) e^{-i\beta_m^-(y-b)} \\ & + b_m \Psi_{ma}^-(\beta_m^-) e^{i\beta_m^-(y-b)} + \bar{b}_m \Psi_{ma}^-(-\beta_m^+) e^{-i\beta_m^+(y-b)}], \end{aligned} \quad (10)$$

and in the stub region II as

$$\begin{aligned} \phi_s = & \sum_m [u_m \Psi_{mh}^+(\gamma_m^+) e^{i\gamma_m^+ y} + \bar{u}_m \Psi_{mh}^+(-\gamma_m^-) e^{-i\gamma_m^- y} \\ & + v_m \Psi_{mh}^-(\gamma_m^-) e^{i\gamma_m^- y} + \bar{v}_m \Psi_{mh}^-(-\gamma_m^+) e^{-i\gamma_m^+ y}]. \end{aligned} \quad (11)$$

Here η_m^\pm , β_m^\pm , and γ_m^\pm are the wavevectors k_m^\pm in regions I, III, and II, respectively. In this paper we study the case where the electron energy is low enough so that at most two modes propagate in the waveguide segments (region I and III) though more modes are considered in the stubs (region II). We proceed as follows.

We match the wave functions of different regions at $y = 0$ and $y = b$: we multiply by $\Psi_{1h}^+(\gamma_1^+)$, $\Psi_{1h}^-(\gamma_1^-)$, $\Psi_{2h}^+(\gamma_2^+)$, and $\Psi_{2h}^-(\gamma_2^-)$, respectively, the equations $\Psi_s(y = 0) = \Psi_1(y = 0)$ and $\Psi_s(y = b) = \Psi_2(y = b)$. Then integrating over x we obtain eight linear equations for the eight coefficients of the wave functions of the two lowest coupled subbands denoted by the matrices $\hat{U}_{12}^T = (u_1, \bar{u}_1, v_1, \bar{v}_1, u_2, \bar{u}_2, v_2, \bar{v}_2)$, in region II, $\hat{L}_{12}^T = (c_1, \bar{c}_1, d_1, \bar{d}_1, c_2, \bar{c}_2, d_2, \bar{d}_2)$ in region I, and by $\hat{R}_{12}^T = (a_1, \bar{a}_1, b_1, \bar{b}_1, a_2, \bar{a}_2, b_2, \bar{b}_2)$ in region III, where T denotes the transfer matrix. This gives

$$\hat{M}_{12} \hat{U}_{12} = \hat{P}_{12} \hat{L}_{12} + \hat{Q}_{12} \hat{R}_{12}. \quad (12)$$

The coefficients corresponding to $n > 2$, $\hat{U}_n^T = (u_n, \bar{u}_n, v_n, \bar{v}_n)$, can be found in a similar way by multiplying by $\Psi_{nh}^+(\gamma_n^+)$ and $\Psi_{nh}^-(\gamma_n^-)$ before integrating over x ; the result is

$$\hat{M}_n \hat{U}_n = \hat{P}_n \hat{L}_n + \hat{Q}_n \hat{R}_{12}. \quad (13)$$

The matrices \hat{M}_{12} , \hat{P}_{12} , \hat{Q}_{12} , \hat{M}_n , \hat{P}_n , \hat{Q}_n as well as the matrices \hat{N}_{12} , \hat{N}_n , \hat{U}_n , $\hat{\eta}_{12}$, $\hat{\beta}_{12}$, appearing in Eqs. (14) and (15), are specified in the appendix.

We now match the derivatives of the wave functions at $y = 0$ and $y = b$ and multiply by $\Psi_{1c}^+(\eta_1^+)$, $\Psi_{1c}^-(\eta_1^-)$, $\Psi_{2c}^+(\eta_2^+)$, $\Psi_{2c}^-(\eta_2^-)$ the equation $d\Psi_s/dy|_{y=0} = d\Psi_1/dy|_{y=0}$ and by $\Psi_{1a}^+(\beta_1^+)$, $\Psi_{1a}^-(\beta_1^-)$, $\Psi_{2a}^+(\beta_2^+)$, $\Psi_{2a}^-(\beta_2^-)$ the equation $d\Psi_s/dy|_{y=b} = d\Psi_1/dy|_{y=b}$. Then we integrate over x and obtain

$$\hat{N}_{12} \hat{U}_{12} + \sum_n \hat{N}_n \hat{U}_n = \hat{\eta}_{12} \hat{L}_{12} + \hat{\beta}_{12} \hat{R}_{12}. \quad (14)$$

Now the relation between the coefficients of the wave function to the left of the waveguide (region I) and to its right (region III) is established as

$$\hat{L}_{12} = (\hat{N}_{12} \hat{M}_{12}^{-1} \hat{P}_{12} + \sum_{n>2} \hat{N}_n \hat{M}_n^{-1} \hat{P}_n - \hat{\eta}_{12})^{-1} (-\hat{N}_{12} \hat{M}_{12}^{-1} \hat{Q}_{12} - \sum_{n>2} \hat{N}_n \hat{M}_n^{-1} \hat{Q}_n + \hat{\beta}_{12}) \hat{R}_{12} = \hat{T}_1 \hat{R}_{12}. \quad (15)$$

If there are more than one unit in the device, we denote the transfer matrix of the i -th stub as \hat{T}_i , that of the i -th waveguide segment as \hat{P}_i , and obtain the total transfer matrix as

$$\hat{T} = \prod_i \hat{T}_i \hat{P}_i. \quad (16)$$

Assuming we input electrons from the left of the device and measure the transmission at its right, the reflection coefficient at its right should be zero. For $E \geq \varepsilon_1^0 = \{E_1 + E_2 - [(\Delta E_{12})^2 + 4\alpha^2\delta^2]^{1/2}\}/2$, with ε_1^0 the first-subband's zero-momentum energy, we have $\bar{a}_1 = \bar{b}_1 = 0$, and for $E \geq \varepsilon_2^0 = \{E_1 + E_2 + [(\Delta E_{12})^2 + 4\alpha^2\delta^2]^{1/2}\}/2$, with ε_2^0 the second-subband's zero-momentum energy, we have $\bar{a}_2 = \bar{b}_2 = 0$. The transmission matrix \hat{M}_t and the reflection matrix \hat{M}_r are given by

$$\hat{M}_t^{-1} = \begin{bmatrix} T_{11} & T_{13} & T_{15} & T_{17} \\ T_{31} & T_{33} & T_{35} & T_{37} \\ T_{51} & T_{53} & T_{55} & T_{57} \\ T_{71} & T_{73} & T_{75} & T_{77} \end{bmatrix}, \quad (17)$$

and

$$\hat{M}_r \hat{M}_t^{-1} = \begin{bmatrix} T_{21} & T_{23} & T_{25} & T_{27} \\ T_{41} & T_{43} & T_{45} & T_{47} \\ T_{61} & T_{63} & T_{65} & T_{67} \\ T_{81} & T_{83} & T_{85} & T_{87} \end{bmatrix}, \quad (18)$$

where T_{ij} is the element of the transfer matrix \hat{T} . The transmission process is then embodied in the matrix \hat{M}_t :

$$\begin{pmatrix} a_1 \\ b_1 \\ a_2 \\ b_2 \end{pmatrix} = \hat{M}_t \begin{pmatrix} c_1 \\ d_1 \\ c_2 \\ d_2 \end{pmatrix} \quad (19)$$

IV. RESULTS AND DISCUSSIONS

In our previous work [7] we obtained a *square-wave* spin transmission as a function of h and d when one mode propagates in the waveguide and the subband mixing due to the SOI is negligible. However, when a gate voltage is applied to the stubs to increase their height h , the second subband approaches the first one and the mixing between them becomes stronger.

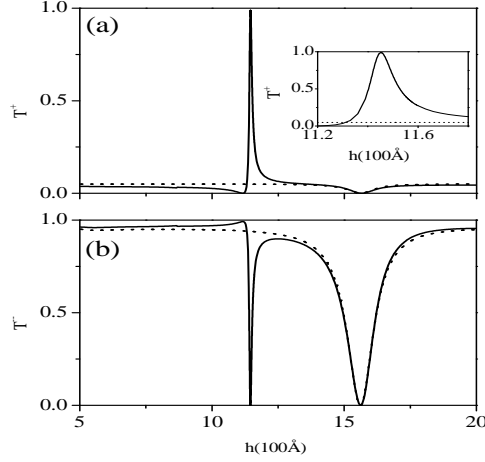


FIG. 3: Transmission T as a function of the stub height h for one stub. Panel (a) is for *spin up* and panel (b) for *spin down*. The solid curves include subband mixing, the dotted ones do not. Notice the absence of the first peak in (a) and the first dip in (b) when mixing is neglected. The inset in (a) is a detailed view of the first peak.

If not otherwise specified, we consider only spin-up incident electrons and the following parameters: width $a = c = 500\text{\AA}$, stub height $h = 1600\text{\AA}$, stub length $b = 660\text{\AA}$, waveguide segment length $l = 1050\text{\AA}$, asymmetry parameter $d = 0$, electron energy $E = 4\text{meV}$, and $\alpha = 1.6 \times 10^{-11} eVm$. The conductance G at zero temperature can be expressed in terms of the transmission T as $G = (e^2/h)T$.

In Fig. 3, we show the spin-up (a) and spin-down transmission (b) through one unit with one symmetric stub as a function of the stub height h when only spin-up electrons are incident. The solid curves denote the results with mixing and the dotted ones without it. The only influence of the mixing in (a) is that a nearly zero transmission is followed by a transmission peak in the range $1100\text{\AA} \leq h \leq 1200\text{\AA}$. The form of the peak is shown in detail in the inset. In contrast, in the same range of h the spin-down transmission in (b) shows a dip instead of a peak. This happens when h has such a value that the first and the second subbands in the stubs are coupled with each other by the mixing term J_{mn} and both of them are coupled well with the waveguide mode through the interface connecting the stub and waveguide. The numerical result shows that the phase of the output electrons is changed by the shift of h when this transmission oscillation happens, which has not been observed when mixing is neglected [7]. Correspondingly, the phase difference between the "+" and "-" branches and the spin orientation of the output electrons is changed by h but the total transmission is kept constant. Here we see that one important effect resulting from

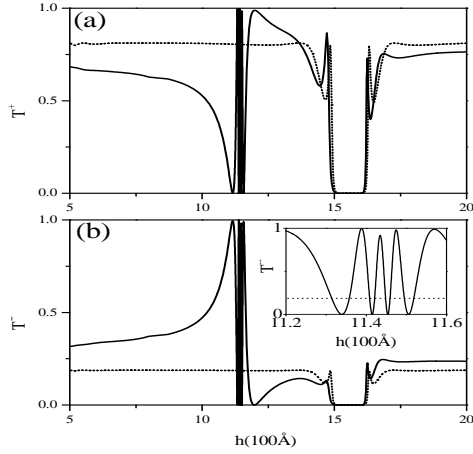


FIG. 4: As in Fig. 3 but for five stubs. Notice the wide gap for both spin states starting at about $h=1500\text{\AA}$. Again the results without mixing (dotted curves) miss the prominent structure near $h=1120\text{\AA}$. The inset in (b) is a detailed view of the region $1120\text{\AA} \leq h \leq 1160\text{\AA}$.

SOI mixing is that the precession of the electronic spins depends not only on the length of the waveguide but also on its shape and width. If we change the parameter α to shift the anticrossing energy E_c , the position of the oscillation does not shift but its amplitude can change. For the parameters used here the electron energy is close to E_c .

Next we evaluate the transmission of a structure composed of five units identical to the one above. We obtain a square-wave pattern of the transmission if we neglect mixing, as shown by the dotted curves in Fig. 4. Surprisingly, the subband mixing does not change the square-wave form of the transmission gap. Nevertheless, both spin-up and spin-down transmissions shift here and there and five oscillations appear for $h = 1120\text{\AA}$. The inset in Fig. 4 (b) shows in detail these oscillations. It is worth noting that here the transmission is much more sensitive to the variation of h than that in the previous one-unit case and its oscillations may be weakened or rounded off by lateral fluctuations of h which are expected to occur in real nanostructures.

Now we fix the height h so that all electrons are reflected: for one stub this happens at $h = 1562\text{\AA}$ and for five stubs at $h = 1600\text{\AA}$. Then we shift the stub along the x direction to change the asymmetry parameter d . The result is shown in Fig. 5 and the mixing effect is negligible. The change in curve order from (a) to (b) is due the change in the length of the structure.

The transmission through one unit versus the electron energy is shown in Fig. 6 for $d = 0$. As in Fig. 3, we observe similar peaks (dips) in the spin-up (spin-down) transmission due

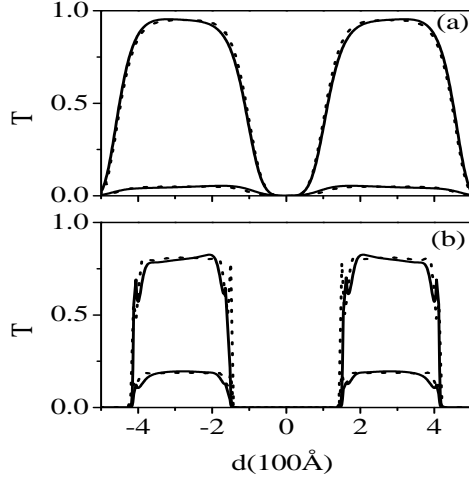


FIG. 5: Transmission T as a function of the asymmetry parameter d for *one* stub in (a) and *five* stubs in (b). The lower (upper) curves in (a) and the upper (lower) ones in (b) are for spin up (down). The solid curves include subband mixing, the dotted ones do not. As shown, the differences between the solid and dotted curves are minimal.

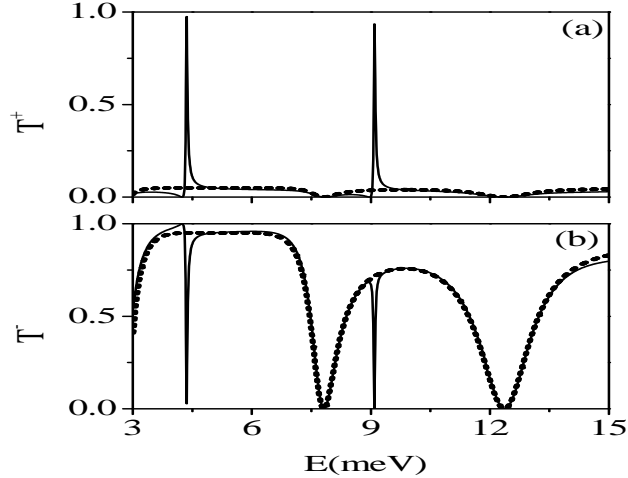


FIG. 6: Transmission T versus incident electron energy for one stub. Panel (a) is for *spin up* and panel (b) for *spin down*. The solid curves include subband mixing, the dotted ones do not.

to the subband mixing and the resulting spin precession. As shown, they occur close to the energies $E = 4.36\text{meV}$ and $E = 9.09\text{meV}$. Apart from these features, the effect of mixing is negligible.

The effect on the transmission, through one stub, when we change both the electron energy E and the asymmetry parameter d , is shown in Fig. 7. In both panels we see the same qualitative behavior between the different curves: we simply notice a shift in the

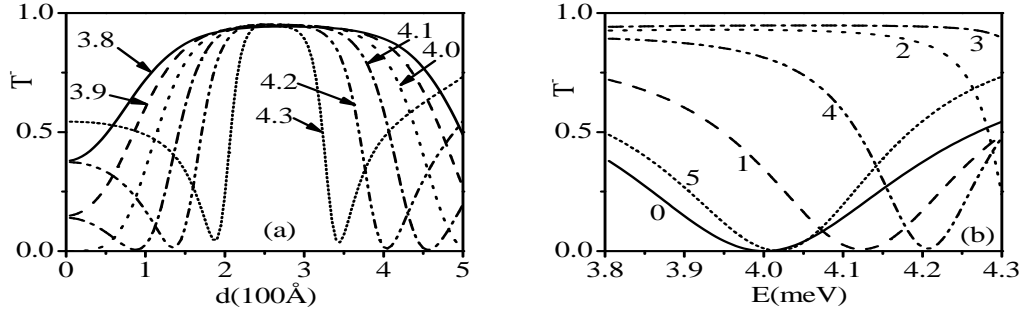


FIG. 7: Spin-down transmission T^- , through one stub, as a function of the asymmetry parameter d in (a) and of the energy in (b). The various curves are marked by the value of the energy (in meV) in (a) and by the value of d (in 100\AA) in (b).

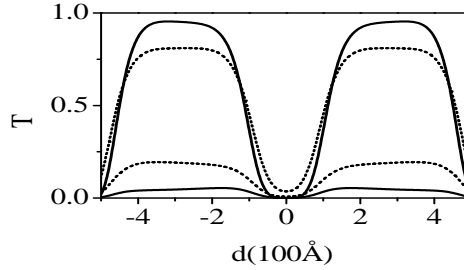


FIG. 8: Transmission T , through one stub, as a function of the asymmetry parameter d for $\alpha = 1.6 \times 10^{-11}$ eVm (solid curves) and $\alpha = 1 \times 10^{-11}$ eVm (dotted curves). The upper (lower) curves are for spin down (up).

minima (gaps) when the two parameters are varied. If we combine several stubs the gaps, e.g., as a function of d , become sharper or take a square-wave form as those in Fig. 5.

Finally, in Fig. 8 we show the dependence of the transmission, through one stub, on the Rashba parameter α . As can be seen, its qualitative behavior remains the same upon changing α . The main change is in the relative contributions to the total transmission of the spin-up and spin-down states. This results from the phase difference $k_y^- - k_y^+$: when mixing is included, Eq. (4), $k_y^- - k_y^+ = 2m^*\alpha/\hbar^2$, is only approximately satisfied, cf. Fig. 2.

V. CONCLUDING REMARKS

We investigated the influence of subband mixing on the spin-dependent electronic transmission through periodically stubbed waveguides in the presence of a weak spin-orbit interaction (SOI). As we saw, the mixing affects mainly the transmission as a function of the incident electron energy and of the stub height and gives rise to the prominent peaks (dips) that are absent when this mixing is negligible. In contrast, the square-wave pattern of the

transmission remains robust when the stubs' degree of asymmetry is varied.

The results we reported were obtained with parameters more easily accessible to experiments than those of Ref. [7]. For instance, the waveguide width is twice bigger and the incident (Fermi) energy four times smaller. We hope that this will further motivate the relevant experiments especially since, as we showed, a weak mixing leaves almost intact the square-wave pattern of the transmission as a function of the stubs' degree of asymmetry.

Though we didn't show any results as a function of the temperature T , we verified and can affirm that the T dependence of the transmission is identical to that reported in Ref. [7]. Finite temperatures T smoothen the curves obtained at $T = 0$. As the ratio $E_F/k_B T$ decreases, the curves are smoothened or rounded off more strongly.

Finally, we also showed that varying the strength of the SOI parameter changes only the relative contribution to the total transmission of the spin-up and spin-down states. Although side gates, needed to control the height h and the distance d , may result in lateral fluctuations, e.g., of h , and though they do not directly address the electron spin, they directly affect the phase of the wave functions in the stubs and accordingly control, through the matching procedure, the transmission profile of either spin orientation. As a result, the nearly square-wave pattern of the transmission can be made more robust if we combine several units. This renders the structure we considered a reasonable candidate for establishing a spin transistor.

Note added in Proof. The journal reviewers brought to our attention Ref. [21] in which the effect of subband mixing, due to the SOI, on the transmission of electrons with energies near the anti-crossing energy E_c was considered in one section of waveguide. The results of this work, obtained in an approximate way, are similar to ours but apply only to a *stubless* waveguide.

VI. ACKNOWLEDGEMENTS

This work was supported by the Canadian NSERC Grant No. OGP0121756.

VII. APPENDIX

Though not appearing explicitly, the product $\langle \Psi_{nw}^\sigma(k) | \Psi_{n'w'}^{\sigma'}(k') \rangle$ in all matrix products mentioned below denotes the integral $\int \Psi_{nw}^\sigma(k, x) \Psi_{n'w'}^{\sigma'}(k', x) dx$, where $\Psi_{nw}^\sigma(x)$ is the wavefunction along x of a waveguide of width w , n is its subband index, k the wavevector, and σ the electron spin. To alleviate the notation we will denote by $(x_1, x_2, \dots) \mathbf{cr}(y_1, y_2, \dots)$ or $(X) \mathbf{cr}(Y)$ the product of the *column* matrix X with the *row* matrix Y .

The upper (4×8) part of the 8×8 matrix \hat{M}_{12} is given by

$$(A_h(\gamma)) \mathbf{cr}(B_h(\gamma)) \quad (A1)$$

where

$$(A_h(\gamma)) = (\langle \Psi_{1h}^+(\gamma_1^+) |, \langle \Psi_{1h}^-(\gamma_1^-) |, \langle \Psi_{2h}^+(\gamma_2^+) |, \langle \Psi_{2h}^-(\gamma_2^-) |) \quad (A2)$$

and

$$(B_h(\gamma)) = (|\Psi_{1h}^+(\gamma_1^+)\rangle, |\Psi_{1h}^+(-\gamma_1^-)\rangle, |\Psi_{1h}^-(\gamma_1^-)\rangle, |\Psi_{1h}^-(-\gamma_1^+)\rangle, \\ |\Psi_{2h}^+(\gamma_2^+)\rangle, |\Psi_{2h}^+(-\gamma_2^-)\rangle, |\Psi_{2h}^-(\gamma_2^-)\rangle, |\Psi_{2h}^-(-\gamma_2^+)\rangle) , \quad (A3)$$

its lower part is

$$(A_h(\gamma)) \mathbf{cr} (|\Psi_{1h}^+(\gamma_1^+)\rangle e^{\gamma_1^+ b}, |\Psi_{1h}^+(-\gamma_1^-)\rangle e^{-\gamma_1^- b}, |\Psi_{1h}^-(\gamma_1^-)\rangle e^{\gamma_1^- b}, |\Psi_{1h}^-(-\gamma_1^+)\rangle e^{-\gamma_1^+ b}, \\ |\Psi_{2h}^+(\gamma_2^+)\rangle e^{\gamma_2^+ b}, |\Psi_{2h}^+(-\gamma_2^-)\rangle e^{-\gamma_2^- b}, |\Psi_{2h}^-(\gamma_2^-)\rangle e^{\gamma_2^- b}, |\Psi_{2h}^-(-\gamma_2^+)\rangle e^{-\gamma_2^+ b}) . \quad (A4)$$

The lower (4×8) part of \hat{P}_{12} (8×8) is zero; its upper part is given by

$$(A_h(\gamma)) \mathbf{cr}(B_c(\eta)) \quad (A5)$$

The upper (4×8) part of \hat{Q}_{12} (8×8) is zero; its lower part is the product

$$(A_h(\gamma)) \mathbf{cr}(B_a(\beta)) \quad (A6)$$

The upper 2×4 part of the matrix \hat{M}_n ($n > 2$) is given by

$$(C_h(\gamma)) \mathbf{cr} (|\Psi_{nh}^+(\gamma_n^+)\rangle, |\Psi_{nh}^+(-\gamma_n^-)\rangle, |\Psi_{nh}^-(\gamma_n^-)\rangle, |\Psi_{nh}^-(-\gamma_n^+)\rangle) , \quad (A7)$$

where

$$(C_h(\gamma)) = (\langle \Psi_{nh}^+(\gamma_n^+) |, \langle \Psi_{nh}^-(\gamma_n^-) |) ; \quad (A8)$$

the lower part is

$$(C_h(\gamma)) \mathbf{cr} \left(|\Psi_{nh}^+(\gamma_n^+)\rangle e^{\gamma_n^{+b}}, |\Psi_{nh}^+(-\gamma_n^-)\rangle e^{-\gamma_n^{-b}}, |\Psi_{nh}^-(\gamma_n^-)\rangle e^{\gamma_n^{-b}}, |\Psi_{nh}^-(-\gamma_n^+)\rangle e^{-\gamma_n^{+b}} \right). \quad (A9)$$

The lower (2×8) part of \hat{P}_n (4×8) is zero; its upper part is given by

$$(C_h(\gamma)) \mathbf{cr} (B_c(\eta)) \quad (A10)$$

The upper (2×8) part of \hat{Q}_n (4×8) is zero; its lower part is the product

$$(C_h(\gamma)) \mathbf{cr} (B_a(\beta)) \quad (A11)$$

The upper 4×8 part of the 8×8 matrix \hat{N}_{12} is given by

$$(A_c(\eta)) \mathbf{cr} (D_h(\gamma)) \quad (A12)$$

where

$$(D_h(\gamma)) = (\gamma_1^+ |\Psi_{1h}^+(\gamma_1^+)\rangle, -\gamma_1^- |\Psi_{1h}^+(-\gamma_1^-)\rangle, \gamma_1^- |\Psi_{1h}^-(\gamma_1^-)\rangle, -\gamma_1^+ |\Psi_{1h}^-(-\gamma_1^+)\rangle, \\ \gamma_2^+ |\Psi_{2h}^+(\gamma_2^+)\rangle, -\gamma_2^- |\Psi_{2h}^+(-\gamma_2^-)\rangle, \gamma_2^- |\Psi_{2h}^-(\gamma_2^-)\rangle, -\gamma_2^+ |\Psi_{2h}^-(-\gamma_2^+)\rangle) \quad (A13)$$

and the lower one by

$$(A_a(\beta)) \mathbf{cr} \left(\gamma_1^+ |\Psi_{1h}^+(\gamma_1^+)\rangle e^{\gamma_1^{+b}}, -\gamma_1^- |\Psi_{1h}^+(-\gamma_1^-)\rangle e^{-\gamma_1^{-b}}, \gamma_1^- |\Psi_{1h}^-(\gamma_1^-)\rangle e^{\gamma_1^{-b}}, -\gamma_1^+ |\Psi_{1h}^-(-\gamma_1^+)\rangle e^{-\gamma_1^{+b}}, \\ \gamma_2^+ |\Psi_{2h}^+(\gamma_2^+)\rangle e^{\gamma_2^{+b}}, -\gamma_2^- |\Psi_{2h}^+(-\gamma_2^-)\rangle e^{-\gamma_2^{-b}}, \gamma_2^- |\Psi_{2h}^-(\gamma_2^-)\rangle e^{\gamma_2^{-b}}, -\gamma_2^+ |\Psi_{2h}^-(-\gamma_2^+)\rangle e^{-\gamma_2^{+b}} \right). \quad (A14)$$

The lower (4×8) part of $\hat{\eta}_{12}$ (8×8) is zero; its upper part is the product

$$(A_c(\eta)) \mathbf{cr} (D_c(\eta)). \quad (A15)$$

The upper (4×8) part of $\hat{\beta}_{12}$ (8×8) is zero; its lower part is given by

$$(A_a(\beta)) \mathbf{cr} (D_a(\beta)). \quad (A16)$$

The upper 4×4 part of the 8×4 matrix \hat{N}_n ($n > 2$) is given by

$$(A_c(\eta)) \mathbf{cr} (\gamma_n^+ |\Psi_{nh}^+(\gamma_n^+)\rangle, -\gamma_n^- |\Psi_{nh}^+(-\gamma_n^-)\rangle, \gamma_n^- |\Psi_{nh}^-(\gamma_n^-)\rangle, -\gamma_n^+ |\Psi_{nh}^-(-\gamma_n^+)\rangle), \quad (A17)$$

and the lower part by

$$(A_a(\beta)) \mathbf{cr} \left(\gamma_n^+ |\Psi_{nh}^+(\gamma_n^+)\rangle e^{\gamma_n^{+b}}, -\gamma_n^- |\Psi_{nh}^+(-\gamma_n^-)\rangle e^{-\gamma_n^{-b}}, \\ \gamma_n^- |\Psi_{nh}^-(\gamma_n^-)\rangle e^{\gamma_n^{-b}}, -\gamma_n^+ |\Psi_{nh}^-(-\gamma_n^+)\rangle e^{-\gamma_n^{+b}} \right). \quad (A18)$$

-
- [1] E-mail: wang@boltzmann.concordia.ca
 - [2] E-mail: takis@boltzmann.concordia.ca
 - [3] J. M. Kikkawa and D. D. Awschalom, Phys. Rev. Lett. **80**, 4313 (1998); *Physics Today*, April 2000, p. 21
 - [4] S. Datta and B. Das, Appl. Phys. Lett. **56**, 665 (1990).
 - [5] E. I. Rashba, Fiz. Tverd. Tela (Leningrad) **2**, 1224 (1960) [Sov. Phys. Solid State **2**, 1109 (1960)].
 - [6] F. Mireles and G. Kirczenow, Phys. Rev. B **64**, 024426 (2001).
 - [7] X. F. Wang, P. Vasilopoulos, and F. M. Peeters, Appl. Phys. Lett. **80**, 1400 (2002); Phys. Rev. B **65**, 165217 (2002).
 - [8] M. Governale, D. Boese, U. Zulicke, C. Schroll, Phys. Rev. B **65**, 140403 (2002).
 - [9] T. Matsuyama, C.-M. Hu, D. Grundler, G. Meier, and U. Merkt, Phys. Rev. B **65**, 155322 (2002); F. Mireles and G. Kirczenow, *ibid* , **66**, 214415 (2002).
 - [10] A. A. Kiseley and K. W. Kim, Appl. Phys. Lett. **78**, 775 (2001).
 - [11] A. V. Moroz and C. H. W. Barnes, Phys. Rev. B **61**, R2464 (2000); *ibid*. **60**, 14272 (1999).
 - [12] M. Governale and U. Zulicke, Phys. Rev. B **66**, 073311 (2002).
 - [13] H. J. Zhu, M. Ramsteiner, H. Kostial, M. Wassermeier, H. P. Schonherr, and K. H. Ploog, Phys. Rev. Lett. **87**, 16601(2001); D. Grundler, *ibid* **86**, 1058 (2001). P. R. Hammar, B. R. Bennett, M. J. Yang, and Mark Johnson, *ibid* **83**, 203 (1999); H. X. Tang, F. G. Monzon, R. Lifshitz, M. C. Cross and M. L. Roukes, Phys. Rev. B **61**, 4437 (2000); L. W. Molenkamp, G. Schmidt, G. E. W. Bauer, *ibid* **64**, R121202 (2001)
 - [14] Y. Ohno, D. K. Young, B. Beschoten, F. Matsukura, H. Ohno, and D. D. Awschalom, Nature **402**, 790 (1999); R. Fiederling, M. Keim, G. Reuscher, W. Ossau, G. Schmidt, A. Waag and L. W. Molenkamp, *ibid* **402**, 787 (1999).
 - [15] L. Loureiro da Silva, M. A. Boselli, X. F. Wang and I. C. da Cunha Lima, Appl. Phys. Lett. **79** 3305 (2001); X. F. Wang, L. Loureiro da Silva, M. A. Boselli, and I. C. da Cunha Lima, Physica E **15**, 23 (2002); M. A. Boselli, A. Ghazali, and I. C. da Cunha Lima, Phys. Rev. B **62**, 8895 (2000); K. Chang, J. B. Xia, and F. M. Peeters, Phys. Rev. B **65**, 155211 (2002); X. F. Wang and P. Vasilopoulos, Appl. Phys. Lett. **81**, 1636 (2002).

- [16] R. Winkler and U. Rössler, Phys. Rev. B **48**, 8918 (1993).
- [17] B. Das, D. C. Miller, S. Datta, R. Reifenberger, W. P. Hong, P. K. Bhattacharya, J. Singh, and M. Jaffe, Phys. Rev. B **39**, 1411 (1989); J. Luo, H. Munekata and F. F. Fang, P. J. Stiles, *ibid* **41**, 7685 (1990).
- [18] J. Nitta, T. Akazaki, H. Takayanagi, T. Enoki, Phys. Rev. Lett. **78**, 1335 (1997); G. Engels, J. Lange, Th. Schapers and H. Luth, Phys. Rev. B **55**, R1958 (1997).
- [19] F. Sols, M. Macucci, U. Ravaioli and K. Hess, Appl. Phys. Lett. **54**, 350 (1989); S. Datta, Superlatt. Microstruct. **6**, 83 (1989).
- [20] H. Wu, D. W. L. Sprung, J. Martorell and S. Klarsfeld, Phys. Rev. B **44**, 6351(1991); R. Akis, P. Vasilopoulos and P. Debray, *ibid* **52**, 2805 (1995); *ibid* **56**, 9594 (1997); P. Debray, R. Akis, P. Vasilopoulos, and J. Blanchet, Appl. Phys. Lett. **66**, 3137 (1995).
- [21] J. C. Egues, G. Burkard, and D. Loss, cond-mat/0209682.